Mon. Not. R. Astron. Soc. **000**, 000–000 (0000) Printed 9 April 1999

Indirect imaging of the accretion stream in eclipsing polars II: HU Aquarii

M.K. Harrop-Allin [1], M. Cropper [1], P.J. Hakala [1,2], C. Hellier [3] & T. Ramseyer [4]

[1] *Mullard Space Science Laboratory, University College London, Holmbury St. Mary, Dorking, Surrey, RH5 6NT, UK*
[2] *Observatory and Astrophysics Laboratory, PO Box 14, FIN-00014 University of Helsinki, Finland*
[3] *Department of Physics, Keele University, Keele, Staffordshire, ST5 5BG, UK*
[4] *Department of Physics and Astronomy, University of Central Arkansas, Conway, AR 72032, USA*

9 April 1999

ABSTRACT

We apply our technique for indirect imaging of the accretion stream to the polar HU Aquarii, using eclipse profiles observed when the system was in a high accretion state. The accretion stream is relatively luminous, contributing as much or more to the overall system brightness as the accretion region on the white dwarf. We model the eclipse profiles using a model stream consisting of a ballistic trajectory from the L1 point followed by a magnetically-channeled trajectory that follows a dipole field line out of the orbital plane. We perform model fits using two geometries: a stream that accretes onto both footpoints of the field line, and a stream that accretes onto only the footpoint of the field line above the orbital plane. The stream images indicate that the distribution of emission along the stream is not a simple function of the radial distance from the white dwarf. The stream is redirected by the magnetic field of the white dwarf at a distance $(1.0\text{–}1.3)\times10^{10}$ cm from the white dwarf; this implies a mass transfer rate in the range $8\text{–}76\times10^{16}\,\mathrm{g\,s^{-1}}$. The absorption dips in the light curve indicate that the magnetically-entrained part of the stream moves from 42° to 48° from the line of centres over the three nights of observation. This is in close agreement with the results of the one-footpoint models, suggesting that this is the more appropriate geometry for these data. The stream images show that in almost all sections of the stream, the flux peaks in B and is successively fainter in U, V and R.

Key words: accretion, accretion discs — binaries: eclipsing — stars: magnetic fields — cataclysmic variables — stars: individual: HU Aqr

1 BACKGROUND

In the strongly magnetic (and thus disc-less) cataclysmic variables, the polars (or AM Herculis stars), the accretion flow from the red dwarf secondary is controlled at large distances from the white dwarf surface by white dwarf's strong magnetic field ($\sim$ 10–240 MG). In these systems, the properties of the accretion flow far from the white dwarf are not well understood. This is because we lack a detailed theoretical understanding of the interactions between the dense stream plasma and the white dwarf's magnetic field, and because emission from the stream is difficult to isolate from other sources of emission in the system, making observational investigations less straightforward. Progress has been made by studying the three main observational signatures of the accretion stream: the strong and variable UV, optical and IR emission lines (e.g. Rosen, Mason & Cordova 1987; Schwope, Mantel & Horne 1997; Šimić et al. 1998); pre-eclipse absorption dips seen in optical and X-ray light curves (e.g. Watson 1995) and optical spectra (Verbunt et al. 1980; Ramsay & Wheatley 1998) of high-inclination systems; and components due to the accretion stream that are seen in the eclipse profiles of several eclipsing polars. Polars that display a bright stream component in their eclipse profiles include UZ For in its high accretion state (Bailey 1995), V2301 Oph (Barwig, Ritter & Bärnbantner 1994, Šimić et al. 1998) and HU Aquarii (Hakala et al. 1993; Schwope, Thomas & Beuermann 1993). The shape of an eclipse profile contains convolved information about the distribution of brightness along the accretion stream.

Hakala (1995) has devised a method based on Maximum Entropy to deduce the distribution of brightness along the accretion stream of HU Aquarii. The method has close parallels with eclipse mapping of accretion discs in non-magnetic systems (e.g. Marsh & Horne 1988) in that both methods use photometric eclipse profiles to deduce the distribution of emission between the component stars, and both make use of Maximum Entropy regularization to constrain the problem. In the accretion stream imaging procedure, one has to assume the trajectory of the accretion stream a priori: the stream trajectory used by Hakala (1995) is an arc connecting the white dwarf (assumed to be a point source) to the L1 point, confined to the orbital plane. We have developed and extended the technique of Hakala (1995) by improving the model's optimizing algorithm and by using a more realistic system geometry and accretion stream trajectory. The improved version of the technique is described in full in Harrop-Allin, Hakala & Cropper (1999, hereafter Paper 1). Tests of the method using synthetic data are presented in Paper 1: we find that the method is able to retrieve information from an eclipse profile in the presence of moderate noise, provided that the phase resolution of the eclipse light curve is good. In this paper we apply this technique to high phase resolution *UBVR* eclipse profiles of HU Aqr obtained when the system was in a high accretion state.

The aim of this study is to deduce the distribution of luminous matter between the secondary star and the white dwarf and to examine the changes in the stream over time and in different wavelengths. The other technique that has been used recently to image the accretion stream is Doppler tomography (e.g. Diaz & Steiner 1994, Schwope et al. 1997, Schwope et al. 1998, Hoard 1999). While Doppler tomography provides an image of the line emission from the accretion flow in velocity space, our method provides an image of the *total* emission of the accretion flow in *spatial* coordinates. The two methods are thus complementary.

2 OBSERVATIONS

We observed HU Aqr during August 1993 when the system was in a high accretion state ($V \sim 15.1$). The data were acquired at a time resolution of 0.2 s (August 17 1993) or 0.1 s (August 18 and 20 1993) using the Stiening high-speed photometer mounted on the 2.1 m reflector at McDonald Observatory, Texas. The Stiening photometer is a four channel instrument enabling the simultaneous acquisition of high-speed photometry in four bands similar to the standard U, B, V and R bandpasses (the incoming light is split using dichroics, and as a result the bandpasses are not standard because the wavelength ranges of adjacent filters do not overlap). A fifth photomultiplier mounted on an offset guider is used to monitor a comparison star. A log of observations is shown in Table 1. The cycle numbers quoted are with respect to the ephemeris in Schwope et al. (1997).

The data were reduced by subtracting the sky background, which was measured approximately every hour. Atmospheric extinction was corrected using extinction coefficients calculated for each the four bands from observations of ten standard stars. The data were binned to a phase resolution of dϕ=0.0001 (approximately 0.72 s) to reduce the noise due to flickering in the out-of-eclipse phases. The high state data contain seven eclipses of which five were considered suitable for application of the modelling technique (the remaining two were spoilt by non-photometric conditions and/or poor guiding). The data were calibrated using the standard star observations. The mean out-of-eclipse magnitudes in each waveband for the three nights are listed in Table 1; these were converted into spectral irradiance using the values quoted in Allen (1973) to enable comparisons between eclipses obtained on different nights and between features in different bandpasses.

3 RESULTS

3.1 The eclipse profiles

Fig. 1 shows the mean light curves in each of the four bands in the (orbital) phase range ϕ =0.79–1.16. The eclipse by the secondary star occurs between phases ~ 0.96 and ~ 1.14, and a pronounced pre-eclipse dip is visible from $\phi \sim 0.83$ to $\phi \sim 0.92$. The eclipse profiles are asymmetric in all four bands, unlike those in low accretion states where the profile is asymmetric in U and R and more symmetric in B and V (Hakala et al. 1993). The eclipse ingress comprises a rapid drop (lasting ~ 5 s in U, ~ 8 s in B and R, and ~ 7 s in V) followed by a more gradual fading to the mid-eclipse level (lasting ~ 130 s in U, ~ 124 s in B and V and 129 s in R). Totality lasts for ~ 445 s in U and R, and

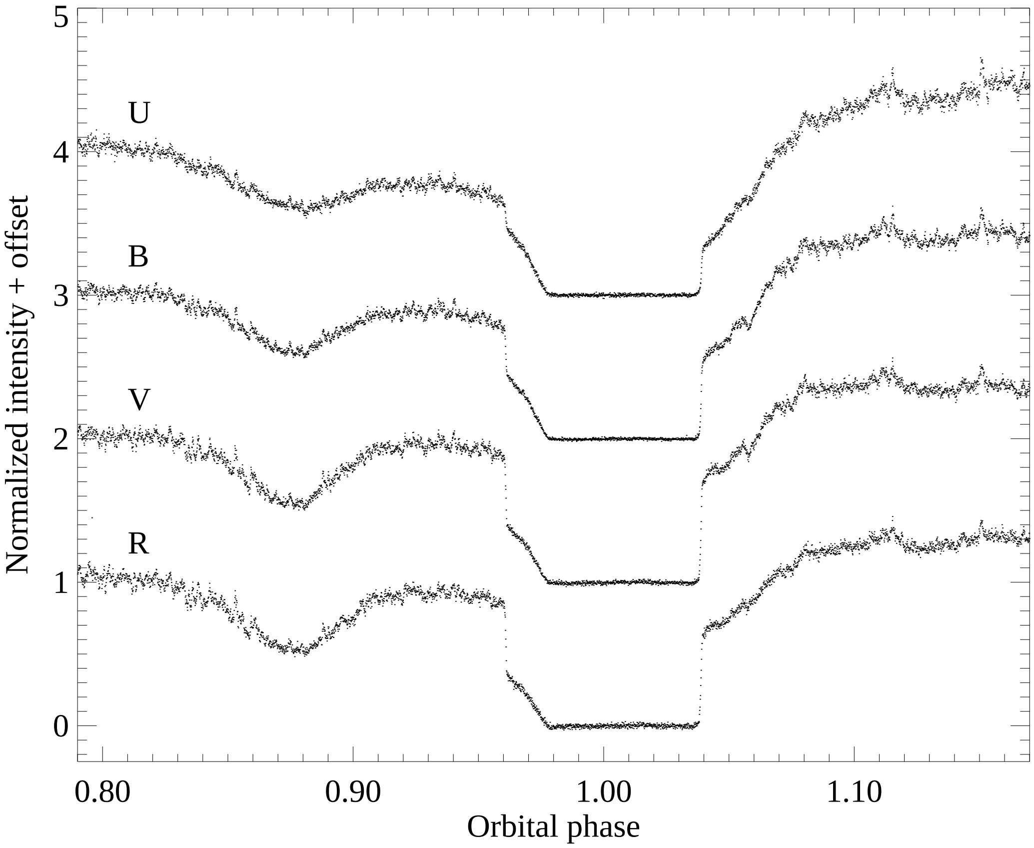

Figure 1. Phase-folded light curves of HU Aqr in a high accretion state for the period 17–20 August 1993. The orbital phase range shown includes the pre-eclipse absorption dip and the eclipse by the secondary star of the accretion region on the white dwarf and the accretion stream. The ordinate is in units of normalized intensity and the V, B and U light curves have been offset by 1.0, 2.0 and 3.0 for clarity.

Table 1. Log of observations: HU Aquarii high-speed photometry

Date	HJD start	Cycle number	Resolution (seconds)	Mean out-of-eclipse magnitude U	B	V	R
17/08/1993	2449216.66614	3688	0.2	14.9	15.0	15.1	15.0
18/08/1993	2449217.63900	3699–3701	0.1	14.8	14.9	15.0	15.0
20/08/1993	2449219.63511	3722–3724	0.1	14.9	15.0	15.1	15.0

~ 451 s in B and V. The components of the eclipse egress are similar: a rapid rise in brightness lasting a few seconds, followed by a more gradual rise to the out-of-eclipse brightness level. The components of the eclipse profile have been identified by Hakala et al. (1993), Glenn et al. (1994) and Schwope et al. (1997): the steep ingress/egress is due to the cyclotron emitting accretion region where the stream impacts on the surface of the white dwarf, while the gradual ingress and egress components are due to the accretion stream. There is no obvious signature of the white dwarf photosphere in the eclipse profile (see later for a discussion). The accretion region is the source of the flickering (occuring on time scales of ~ 5 s) in the light curve: once the accretion region has been eclipsed (at $\phi \approx 0.962$), the stream ingress is free from flickering noise. The flickering variations of the accretion region probably indicate a non-homogeneous accretion flow incorporating denser blobs of material.

The eclipse width $\Delta\phi$ (measured here as the phase duration of the eclipse of the accretion region) is remarkably stable, not just throughout the duration of the high state data, but also between our high and previous low state data. The mean value in the high state is $\Delta\phi = 0.0779 \pm 0.0002$ and is consistent with that in the low state: $\Delta\phi = 0.078 \pm 0.001$ (measured from data in Hakala et al. 1993). These measurements are also consistent with that of Schwope et al. (1997) who report an eclipse width of 584.6 s (corresponding to $\Delta\phi = 0.0779$) from observations taken contemporaneously with our high state data.

The shape of the stream ingress component shows slight variations from cycle to cycle. If these changes are due to a non-uniform distribution of emission along the accretion stream, we expect these changes to correspond to changes in the stream brightness distributions (see section 4.2). The *duration* of the stream ingress, on the other hand, is constant in a given waveband. This is in contrast to the dramatic variability observed by Glenn et al. (1994) where the accretion stream ingress duration increased by approximately one minute between two successive eclipses.

The relative brightnesses of the stream and accretion region components are functions of wavelength and of the accretion state of the system. Our calibration of the high state data allows us to compare directly the brightness of the stream and the accretion region between the four bands; the measurements of the brightnesses of the stream and spot components during the eclipse ingress are listed in Table 2. Table 2 also lists the ratio between the stream and the spot component fluxes in the four wavebands in both the high and the low state. In the high state, both the stream and the accretion region are brightest in B, while the accretion region is faintest in U and R, and the stream is faintest in R. The brightness of the accretion region in the four bands is roughly that expected for cyclotron emission in a magnetic field of ~ 37 MG (as calculated for HU Aqr by Schwope et al. 1993 and Glenn et al. 1994), since the cyclotron intensity is expected to peak in the 4-6th harmonics (Wickramasinghe & Meggitt 1985).

In the high state the stream's contribution to the total emission in each of the four bands is comparable to, and in U and B exceeds, the emission from the accretion region. In the low state, the stream is comparable in U to the accretion region. The fact that the stream contributes significantly to the system emission was stressed by Hakala et al. (1993) and Hakala (1995). HU Aqr is not the only system with a bright accretion stream in the optical. The unfiltered high state eclipse profile of UZ For in Bailey (1995) has an stream component that contributes approximately 55 per cent of the pre-eclipse brightness. The eclipse profiles of V2301 Oph presented in Barwig et al. (1994) also show bright stream components: the contributions to the out-of-eclipse level are ~ 53 per cent in U, B and V, and ~ 57 per cent in R.

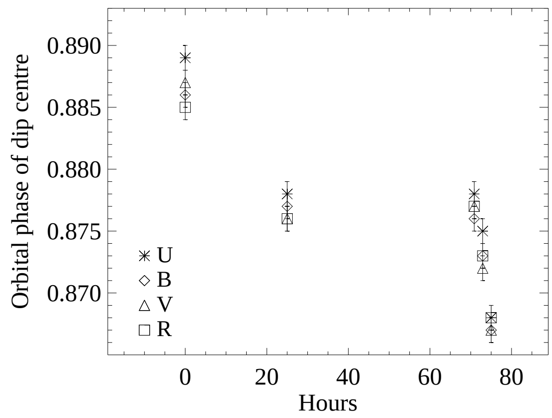

Figure 2. The variation in phase of the centre of the pre-eclipse dip at $\phi \sim 0.88$ with time and with wavelength. The horizontal axis shows time since mid-eclipse of cycle 3688. The dip occurs at increasingly earlier phases as the run progresses, and in each cycle occurs latest in U.

We examined our eclipse profiles for signs of the eclipse of the white dwarf photosphere, since features caused by the white dwarf have been seen in other eclipsing polars (e.g. UZ For: Bailey & Cropper 1991). The best place to look for a white dwarf photosphere component is in the phase range $1.038 \lesssim \phi \lesssim 1.039$ before the accretion spot egress. The relative duration of the photosphere component before the spot egress to that afterwards is determined by the position of the accretion region on the white dwarf. We estimate that the photosphere component before the spot egress would last at least ~ 12 s (using parameters discussed in section 4.1). Close inspection of our eclipse profiles reveals that the longest possible duration for a photosphere component at these phases is ~ 6 s in U, and shorter in the other wavebands. We thus conclude that there is no significant white dwarf photosphere component in the eclipse profiles, and that we may safely omit this from our models.

A persistent feature in the eclipse profiles occurs at $\phi \approx 0.970$ in all four wavebands. This is a change in gradient during the stream ingress component, which is caused by the non-uniform distribution of emission along the stream. We explore this issue in section 4.2 when we determine the stream brightness distributions.

3.2 The pre-eclipse dip

HU Aqr shows a conspicuous pre-eclipse dip in all four bandpasses (see Fig. 1). Using Gaussian fits, we find that the dip centre changes noticeably over the course of the run, moving to increasingly earlier phases as the run progresses: in cycle 3688, the

Table 2. Mean spectral irradiances of the stream and the spot components during high state eclipse ingress (the uncertainties quoted are 1-sigma errors), and the ratio of the fluxes of the stream to the spot flux. For comparison, the ratio of the stream flux to the spot flux in the low accretion state is listed; these values are taken from Hakala et al. (1993).

	spot (10^{-15} erg cm^{-2} s^{-1} Å^{-1})	stream (10^{-15} erg cm^{-2} s^{-1} Å^{-1})	high state ratio (stream/spot)	low state ratio (stream/spot)
U	0.6 ± 0.2	2.00 ± 0.02	~ 3.3	~ 0.67
B	2.0 ± 0.4	2.5 ± 0.2	~ 1.3	~ 0.19
V	1.6 ± 0.2	1.2 ± 0.1	~ 0.75	~ 0.03
R	0.8 ± 0.1	0.52 ± 0.08	~ 0.65	~ 0.45

dip centre occurs at $\phi \approx 0.883$ while in cycle 3724 the dip centre has moved to $\phi \approx 0.867$, a difference of approximately two minutes. Fig. 2 shows this trend (the uncertainties on the dip centre measurements represent the 99 per cent confidence level derived using the method of Lampton, Margon & Bowyer 1976). This change in phase corresponds to a change in azimuth of the absorbing material from 42° to 48° from the line of centres. Schwope et al. (1997) find the centre of the absorption dip at $\phi = 0.882 \pm 0.003$ measured from phase-folded B-band data from the period 16–18 August 1993, immediately preceding our observations. There appears to be no time-dependent variation in the 1-sigma width of the dip within our data. The dip width is consistently largest in U, and then similar in the other wavebands.

4 INDIRECT IMAGING OF THE ACCRETION STREAM

4.1 Details of the model

4.1.1 The optical depth of the stream

We assume that the stream is predominantly self-luminous, and that the emission from each point is modulated only by the viewing angle to that point. Further degrees of freedom are difficult to justify: for example, if one assumes that the stream emission is bright on the side facing the white dwarf and dark on the side that is not irradiated by the white dwarf, this implies that the only excitation mechanism in the stream is photoionization by the high energy radiation from the white dwarf. There are, however, many other heating mechanisms that could be operating in accretion streams — see Harrop-Allin (1999) for a discussion. Better data may be sufficient to constrain more complex emission patterns from the stream, but for the moment we assume a cylindrical symmetry with a simple projection factor (equal to the sine of the angle between the line of sight and the tangent to the stream at each point) as a first approximation to the optical depth of the stream.

4.1.2 Accretion onto one or both poles?

Before the imaging procedure can be applied we need to specify whether the the stream accretes onto one or onto both footpoints of the field line. In the case of HU Aqr, we find evidence for both one and two-pole accretion in the high state. On the one hand, the overall shape of the high state light curve is consistent with cyclotron beaming from a single pole (Schwope et al. 1994); also, Schwope et al. (1998) claim that HU Aqr has not shown signs of a second active pole.

On the other hand, optical circular polarimetry (Hakala, unpublished data) obtained in June 1993 shows large negative (~ -7 per cent) and smaller positive (~ 3 per cent) excursions during the orbital period. Although these polarization observations were not made contemporaneously with our data, we notice that the overall shape of the intensity light curve in June 1993 is very similar to the shape of our high state light curves from August of the same year (and is also similar to the high state light curves of Schwope et al. 1994 and Schwope et al. 1997). We have therefore performed model fits to our eclipse profiles using both one- and two-footpoint geometries.

4.1.3 Choosing the fixed parameters

The parameters that are fit by the optimizing algorithm are the brightnesses of the emission points along the stream. For each model fit, there are a number of parameters that are fixed (see Paper 1 for full details). These are physical parameters such as the primary mass M_1, the radius R_μ at which the accretion stream couples onto the magnetic field, the brightness of the accreting pole(s) and the mass ratio q of the system; and geometric parameters such as the binary inclination i, the magnetic co-latitude β of the dipole field, and its longitude ζ. Fortunately, estimates of many of these parameters are available from previous studies, and these were used as a basis for the fixed parameters. The fixed parameters were determined by varying their values by hand until acceptable fits were found. In some cases small changes from the published values were found to produce slightly better fits; these parameters were adopted accordingly.

We took our value for the primary mass from Glenn et al. (1994), who find $M_1 \approx 0.9\,M_\odot$ (we used $M_1 = 0.9\,M_\odot$ in all our models). The values for i and q together determine the phase width between the steep components due to the accretion region. Using $i = 85°$ (Glenn et al. 1994, Schwope et al. 1993, Schwope et al. 1997), we found that the eclipse widths were well-reproduced when $q = 0.252$. This is in agreement with the range of values for q determined by Hakala et al. (1993): their figure 8 implies a mass ratio $0.2 < q < 0.4$ for $80° < i < 85°$. Also, Schwope et al. (1997) deduce $q = 0.25$ from their model of the narrow component of the optical emission lines in HU Aqr. We used $i = 85°$ and $q = 0.252$ for all our model fits.

The quantities R_μ, β and ζ affect primarily the duration of the stream ingress and egress components in the model light curves. We took as our starting point the value of β from Schwope et al. (1997), who find that the structures in Doppler tomograms of the main optical emission lines are consistent with $\beta = 25°$. For the two-footpoint geometry models and β in the range $23° \leq \beta \leq 27°$ we found acceptable fits for $0.21\,a \leq R_\mu \leq 0.23\,a$, where a is the orbital separation of the two stars. We note that Schwope et al. (1997) find values for the coupling radius in the range $0.20\,a \leq R_\mu \leq 0.29\,a$ (as measured from their figure 14).

In the one-footpoint geometry models, the duration of the stream components is not quite as sensitive to the value of β as is the case in the two-footpoint models. Changes of up to 5° from 30° (used for all one-footpoint model fits) do not alter noticeably the duration of the stream components. The duration of the stream ingress is, however, very sensitive to changes in R_μ for this geometry. The values for R_μ are smaller than in the two-footpoint model, and fall into the range $0.17a \leq R_\mu \leq 0.20a$ for the five eclipses.

We found by trial and error that values for β and R_μ outside the above ranges significantly reduce the quality of the fits. The quality of the fits is not, however, very sensitive to the values chosen for ζ, and we used 10° throughout (for both geometries). Values in the range $0° \leq \zeta \leq 30°$ produce similar fits; values of ζ outside this range produce stream ingress and egress durations in the models which are noticeably different from those in the data.

4.1.4 Weights assigned to the light curve

We have assigned weights to the data according to the structures in the eclipse profile at various phases. At phases earlier than 0.891 and later than 1.128 the model stream is fully visible. During these phases, there is no information in the shape of the profile to establish the relative brightnesses of the emission points along the stream. We therefore assign small weights to the light curve during these phases. At $\phi = 0.891$, points along the free-fall part of the stream near the L1 point begin to be eclipsed. The accretion region is eclipsed during $0.960 \lesssim \phi \lesssim 0.962$, and the light curve is free from flickering noise from here until eclipse totality. During the stream ingress, we use the small uncertainties from the phase binning of the original data (i.e. the standard deviation of points in each 0.0001 phase bin). During $1.038 \lesssim \phi \lesssim 1.040$ the accretion region emerges, whereafter the stream emerges, becoming fully visible by $\phi \approx 1.128$.

We assign small weights to the narrow phase intervals where the accretion region is eclipsed. This is because the steep changes in the eclipse profile are not instantaneous, whereas the model assumes that the accretion regions are point sources and that their eclipses are instantaneous. A very slight misalignment between the model curve and data points on the steep component of a real eclipse profile would result in spuriously poor fit at this phase. We assign small weights in these phase ranges to prevent the fit from being dominated by the steep components where there is no useful information about the distribution of emission along the stream. During the stream egress, we have to assign weights that are sufficiently small to prevent the model from fitting the flickering, but large enough so that underlying shape of the light curve is preserved. To do this we calculate a running average over 50 points ($\Delta\phi = 0.005$) and use the mean of the residuals between the original brightnesses and the running average as an estimate of the uncertainty at each point.

4.2 The stream brightness distributions

4.2.1 Two-footpoint geometry

Fig. 3 shows the results of the imaging procedure for the eclipse profiles of cycle 3724, using a model stream that accretes onto both footpoints of a dipole field line. The parameters used for these fits were $\beta = 25°$, $\zeta = 10°$ and $R_\mu = 0.22\,a$ (approximately 20 white dwarf radii). The quality of the fits can be assessed by examining the value of the "fitness function" F (used in the optimizing algorithm; see equation 1 in Paper 1), which we know from simulations in Paper 1 should be $\lesssim 3000$ for this phase resolution and noise level. The fit to the U-band eclipse has $F = 2394$, and the B, V and R fits have F equal to 2592, 2630 and 2617 respectively.

The range of values of R_μ ($0.21\,a \leq R_\mu \leq 0.23\,a$) found for the five eclipses using the two-footpoint geometry implies an angle between the magnetic part of the stream and the line of centres

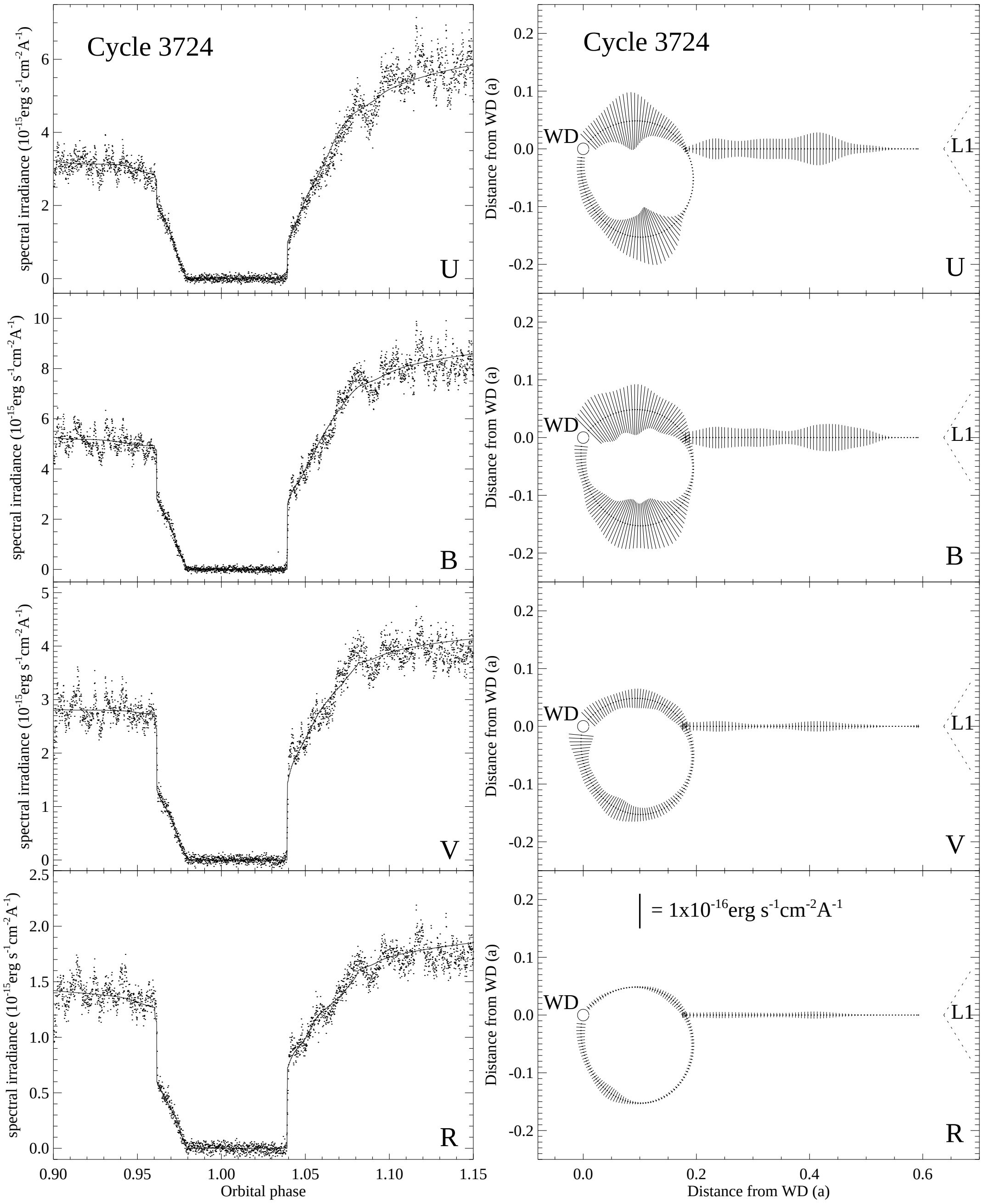

Figure 3. Model eclipse profiles and the corresponding images of the accretion stream for cycle 3724, using a stream that accretes onto both footpoints of a dipole field line. The stream images are shown projected onto the plane perpendicular to the orbital plane and passing through the centre of both stars. The brightness of each emission point is shown as a line through the point, perpendicular to the stream; the length of each line indicates the brightness of the point. The white dwarf is shown to scale as a circle (labelled 'WD'), and the secondary is shown (not to scale) to mark the position of the L1 point (labelled 'L1').

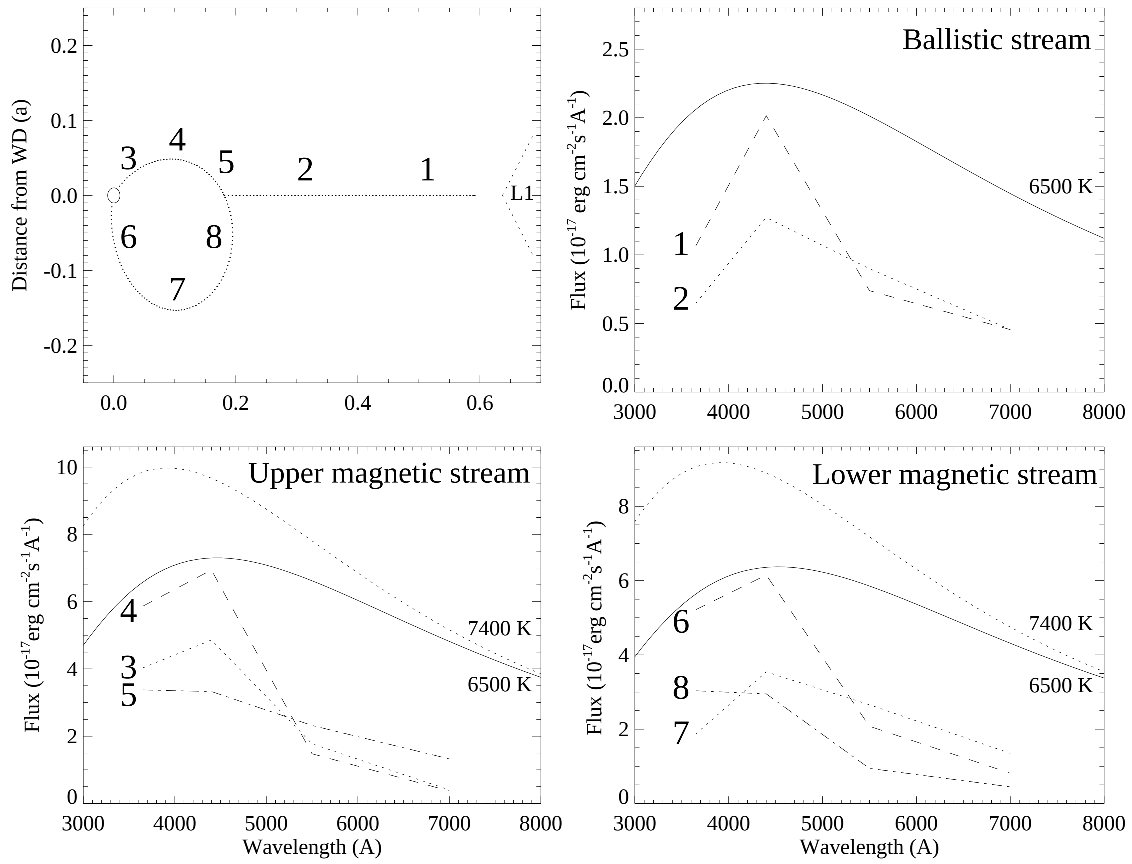

Figure 4. The colour-dependence of the stream brightness distributions for cycle 3723 (similar results are found for the other four cycles). The stream is divided into eight sections (top left panel) and the average flux per stream emission point in each section is plotted in the four wavebands for each of the eight sections of the stream. In most stream sections, the peak flux occurs in B. However, in sections 5 and 8, immediately adjacent to the coupling radius on the magnetically-channeled portion of the stream, the fluxes in U and B are comparable. Blackbody curves for temperatures of 6500 K and 7400 K are shown for illustration.

in the range 39–41°. There appear to be no systematic trends in the variations of R_μ over the course of the observations.

The geometric parameters of the model describe a magnetic field geometry and an orbital inclination such that the lower accreting pole (i.e. the pole on the opposite side of the orbital plane as the observer) is occulted by the white dwarf throughout the phases of interest. As a result, the only way in which the brightness chosen for the lower pole itself influences the stream model is due to the enforced continuity (by the regularisation term in the optimizing function: see Paper 1) with the stream emission points in its immediate neighbourhood. The steep components in the eclipse profiles and in our model fits are produced by the upper pole only. For these reasons, the value used for the fractional lower pole brightness, 0.10, is not constrained by the model. There are no obvious trends with time in the upper pole brightnesses in a given waveband.

There are several common features in the stream brightness distributions in the four wavebands and the five cycles spanned by our data. The emission is clearly not uniform along the stream, nor is it a simple function of the radial distance from the white dwarf. Rather, there are regions of the stream with localised brightness enhancements, particularly within the magnetosphere. In all model streams there is very little emission on the lower half of the magnetic part of the stream immediately below the orbital plane. There is, however, a very bright and fairly compact region on this half of the stream closer to the white dwarf. This is a persistent feature in the two-footpoint stream models in all cycles and can be seen clearly in Fig. 3, especially in the U image. Interestingly, there is no

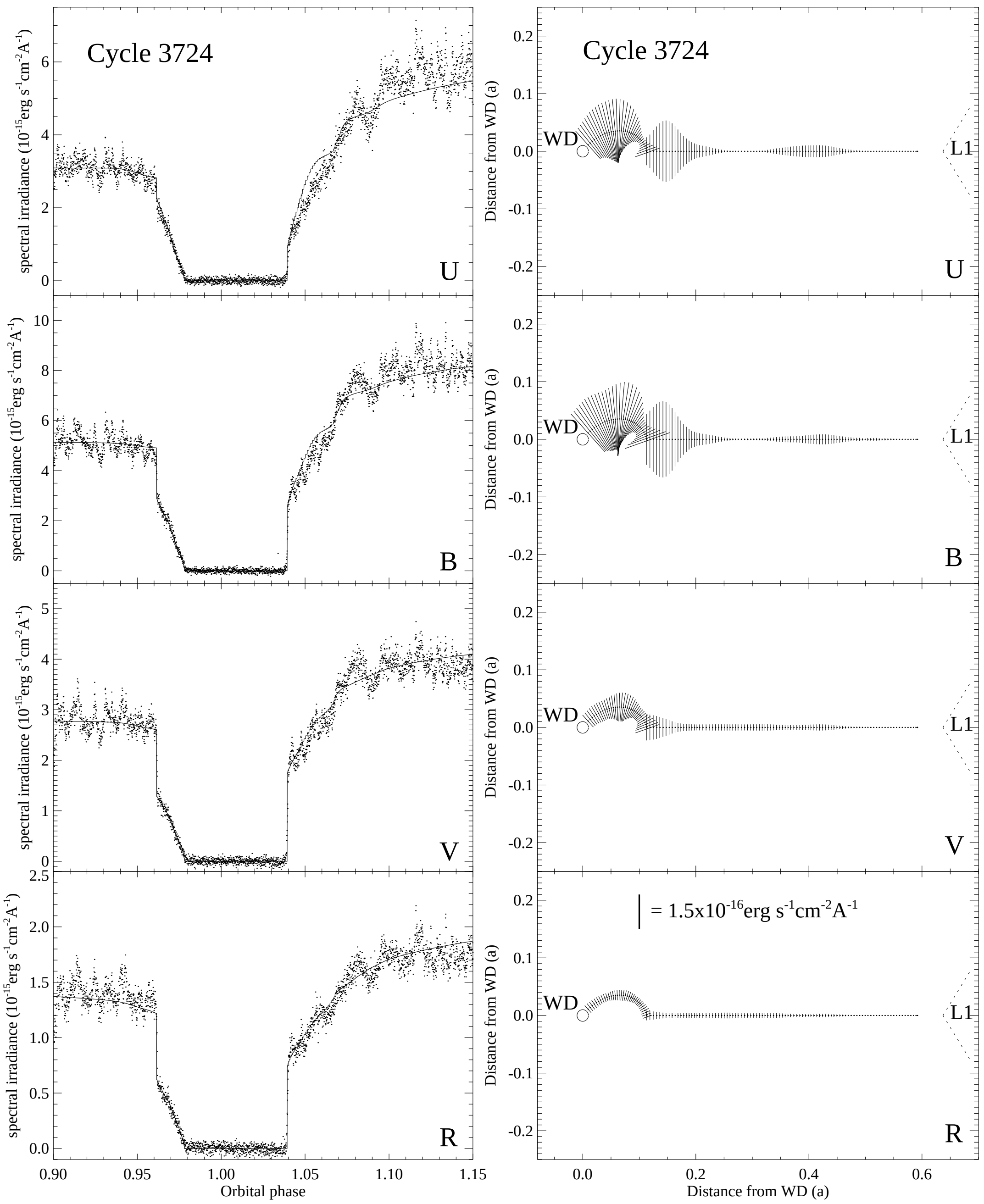

Figure 5. As for Fig. 3, but for a model stream that accretes onto only the footpoint of the field line above the orbital plane (on the same side of the orbital plane as the observer).

obvious brightening of the stream as it approaches either R_μ or the white dwarf.

To investigate the colour dependence of the stream images, we divide the stream into eight sections and the average flux per stream emission point in each section is examined in turn. The ballistic stream is divided into two sections (of equal length), while the magnetic stream above and below the orbital plane is divided into three sections each (see Fig. 4). In all stream sections apart from the two sections on the magnetic field line immediately adjacent to R_μ, and all cycles, the stream flux (in $\mathrm{erg\,cm^{-2}\,s^{-1}\,\AA^{-1}}$) is highest in B and successively lower in U, V and R. In four of the five cycles, the stream flux is comparable in U and B in the two sections of the stream adjacent to R_μ (labelled '5' and '8' in Fig. 4). A possible explanation for this is outlined in section 5.4.

4.2.2 One-footpoint geometry

Fig. 5 shows sample results (for cycle 3724) using a stream that accretes onto the footpoint of the field line above the orbital plane only. The fits in the figure have $\beta = 30°$, $\zeta = 10°$ and $R_\mu = 0.17$. The values of the fitness function F for these fits are 2859, 2895, 2773 and 2938 for U, B, V and R respectively.

There are no obvious trends in the fractional brightness of the accretion region with time in a given waveband. The R_μ values, however, show a clear trend. As the run progresses, the R_μ values steadily decrease. The fit for cycle 3688 requires $R_\mu = 0.20$ and the fit for cycle 3724 has $R_\mu = 0.17$. This corresponds to an increase in the angle between the magnetic part of the stream and the line of centres from 42° to 47°.

The stream images for the one-footpoint geometry are quite different from the two-footpoint geometry results. There is very little emission from the ballistic stream in all cycles. The stream brightens as it approaches R_μ in all four wavebands. As the stream leaves the orbital plane it fades, and brightens once again as it approaches the accretion region. The brightest part of the stream is not, however, always closest to the white dwarf, but occurs in U and B in cycles 3688, 3723 and 3724 about $0.08\,a$ from the white dwarf. We examined the wavelength dependence of the stream brightnesses as before by dividing the stream into sections; for this geometry we divided both the ballistic stream and the magnetic part of the stream into two sections. In all cycles and in all four sections of the stream the flux is highest in B, and is successively lower in U and V and lowest in R.

The values of the fitness function for the fits produced by the one-footpoint geometry are larger than those for the two-pole geometry fits, although it could be argued that this is simply because there

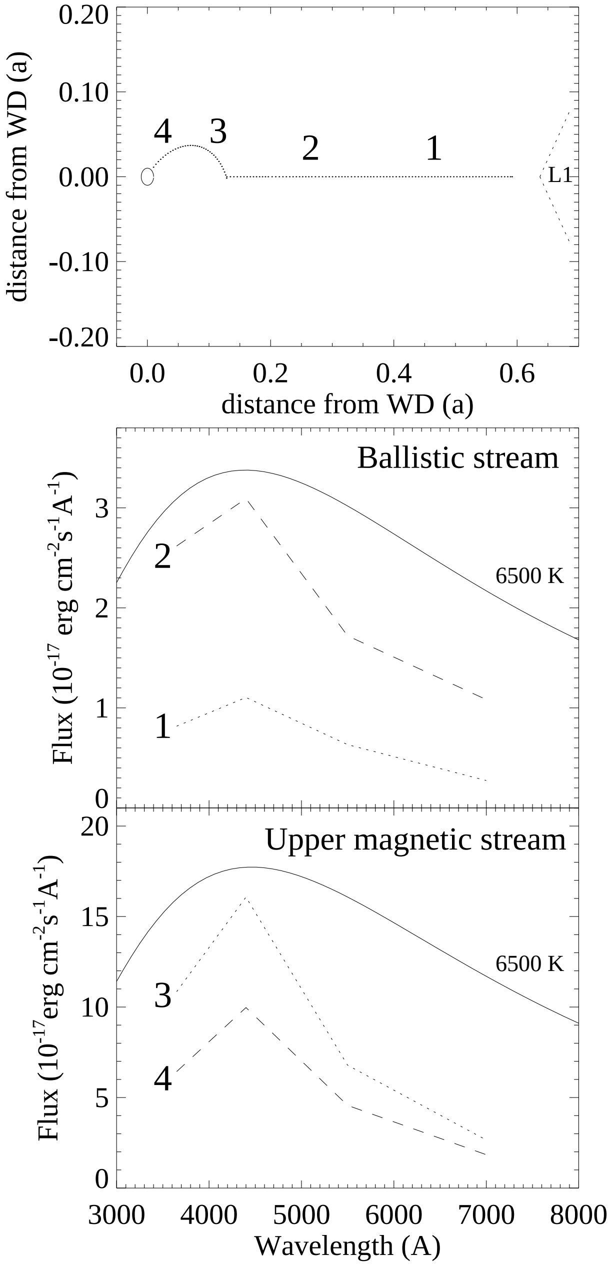

Figure 6. The colour-dependence of the stream brightness distributions for cycle 3722 (similar results are found for the other four cycles). The stream is divided into four sections (top panel) and the average flux per stream emission point in each section is plotted in the four wavebands for each of the four sections of the stream. In all stream sections, the peak flux occurs in B. A blackbody curve for a temperature of 6500 K is shown for illustration.

are more parameters in the two-footpoint model. It is not straightforward to establish which of the two geometries produces a better fit: the application of an F-test to distinguish between the two models on statistical grounds is problematical because the quantity that is minimized is not χ^2, but χ^2 plus a maximum entropy regularization term (for full details see Paper 1). In addition, an F-test would be affected by the weights adopted for the different phase ranges in the light curve (section 4.1.4).

5 DISCUSSION

5.1 The absorption dip and the movement of the stream

Absorption dips in polar light curves are thought to originate at phases where the magnetically-channeled portion of the accretion stream occults the emission region on the white dwarf (see e.g. Watson 1995 for a review). The dip in HU Aqr at $\phi \sim 0.88$ is almost certainly caused by absorption in the stream. First, HU Aqr has the necessary accretion geometry to produce such a dip: the condition $\beta < i$ (see e.g. Watson 1995) is satisfied since HU Aqr has $\beta \approx 26°$ and $i \approx 85°$ (Glenn et al. 1994, Schwope et al. 1997, this work). Secondly, the depth of the dip in a given wave-band is similar to the depth of the steep component during eclipse ingress, suggesting that the dip is caused by the occultation of the accretion region emission. The evidence is strengthened by the fact that the strong optical emission lines in HU Aqr, which are thought to originate in the accretion stream (e.g. Liebert & Stockman 1985), are not occulted during the dip (Schwope et al. 1997). The observed variation of the phase of the centre of the absorption dip (Fig. 2) has implications for the accretion flow: the absorbing material in the accretion stream moves from an azimuth of 42° to 48° from the line of centres on a time scale of a few days. This is evidence for the variable nature of the interaction between the stream and the magnetic field of the white dwarf.

Given that the absorbing material is located in the magnetically-confined part of the stream, the range of angles predicted by the pre-eclipse dip should correspond to the range of angles between the magnetically-entrained part of the stream trajectory and the line of centres as predicted by the stream models. The range predicted by the two-footpoint models is 39–41°, quite distinct from the range predicted by the dips; in addition, there is no obvious trend to larger angles with time.

The one-footpoint models, on the other hand, show a remarkable agreement in both the trend of decreasing R_μ and the range of predicted angles (42°–47°). This agreement suggests that the one-footpoint geometry is the more appropriate for these data. The original motivation for trying the two-footpoint geometry to model the eclipses was that circular polarization of HU Aqr in the high state shows both positive and negative excursions. However, it should be remembered that the polarimetry was not contemporaneous with these data. Furthermore, it could be argued that the excursions of opposite sign in the circular polarization could be the result of viewing a tall accretion column from below.

It is tempting to try to link changes in R_μ and the azimuth of the magnetically channeled part of the stream to changes in the mass transfer rate in the stream, and thus to the overall brightness of the system. However, the mean out-of-eclipse magnitudes over the run are constant to within the measurement uncertainties (about 0.1 mag), so there are no obvious changes in the overall brightness of the system. A similar effect was observed by Schwope et al. (1998) in *ROSAT* HRI data of HU Aqr, where the azimuth of the magnetically-confined part of the stream moves by $\sim 17°$ without an obvious change in the HRI count rate.

5.2 Comparison with Doppler tomograms

The Doppler tomograms of HU Aqr in Schwope et al. (1997) were calculated using optical spectra obtained almost simultaneously with our high-speed photometry. This provides an opportunity to make a comparison between the tomograms and our images of the stream, with the caveat that the tomograms are images of line emission in velocity space, whereas our results are images of the total emission in spatial coordinates.

There are two main structures in the tomograms that Schwope et al. (1997) attribute to the accretion stream (see their figure 12). First, there is a bright 'cometary' tail which is identified as emission from the ballistic stream. The second feature is a faint smeared region at negative velocities which represents emission from material in the magnetosphere of the white dwarf.

A comparison between our images and the tomograms shows that *line emission is not the dominant emission mechanism in the stream.* While it may be difficult to relate the apparent flux in the tomogram to the emitted line flux, it is clear in the tomograms that the integrated flux in the velocity space appropriate to the ballistic stream exceeds that from the magnetically-channeled stream. Looking at our B-band images in Fig. 3 and Fig. 5, we see the reverse: the emission from the magnetically-channeled part of the stream dominates the emission from the ballistic stream. The line flux is thus a small fraction of the total optical emission from the stream.

The large ratio of total (line plus continuum) stream emission to stream line emission (in the optical) can also be seen in optical spectra. We have estimated the ratio of line to continuum emission in the high state using the mean spectrum in Schwope et al. (1997) (we have used our mean out-of-eclipse magnitudes to estimate the continuum level, as the spectrum presented in Schwope et al. (1997) is continuum-subtracted). The ratio of continuum emission to line emission is ~ 8 in the B-band. The fraction of the continuum due to the *stream* (as opposed to cyclotron emission from nearer the white dwarf) can then be estimated using the figures in Table 2; we see that approximately 56 per cent of the pre-eclipse light level is due to the stream. This implies that the stream continuum flux exceeds the line emission flux by a factor of ~ 4.3 in the high state. The corresponding measurement in the low state, using the spectrum in Hakala et al. (1993), shows that even in reduced accretion states the continuum flux from the stream exceeds the line flux by a factor of 2.5 in B.

5.3 The mass transfer rate

If we assume that R_μ is the radius at which the ram pressure of the stream is balanced by the magnetic pressure of the white dwarf field, we can use our values of R_μ to estimate the mass transfer rate in the stream via the equation

$$R_\mu = 1.45 \times 10^{10} \mu_{34}^{4/11} {\sigma_9}^{4/11} {M_1}^{-1/11} \dot{M}_{16}^{-2/11}\,\mathrm{cm} \quad (1)$$

(Mukai 1988, Warner 1995), where μ_{34} is the magnetic moment of the white dwarf in units of $10^{34}\,\mathrm{G\,cm^3}$, σ_9 is the radius of the stream in units of 10^9 cm and $\dot{M}_{16}$ is the mass transfer rate in units of $10^{16}\,\mathrm{g\,s^{-1}}$. This equation assumes that the incoming stream does not distort the magnetic field of the white dwarf and that the threading of the stream is instantaneous. For HU Aqr we have $M_1 \approx 0.9\,M_\odot$, $\mu_{34} \approx 0.8$ and $B \approx 37$ MG. To estimate the radius of the stream, we use the width of the pre-eclipse absorption dip (e.g. Watson et al. 1995). Since the inclination is high,

$$\sigma \approx \pi\, d\, \Delta\phi / \sin i \quad (2)$$

where d is the distance from the white dwarf to the absorbing material in the stream. The absorption dips have $\Delta\phi \approx 0.080$. We make the assumption that the absorption occurs at a distance of R_μ, since i is near 90°. Equation 2 then implies $\sigma_9 \approx 3.0$. This is comparable to values of the stream radius from Lubow & Shu (1975) where $\sigma_9 \sim 1$. Using $\sigma_9 = 3.0$, we find that the range in R_μ predicted by the stream models imply $\dot{M}$ in the range 8–$76 \times 10^{16}\,\mathrm{g\,s^{-1}}$.

This result is quite sensitive to the value of σ_9, since $\dot{M} \propto \sigma^2$. For example, if $\sigma_9 = 1$, the implied mass transfer rate is reduced to $(1-5) \times 10^{16}\,\mathrm{g\,s^{-1}}$. Heerlein et al. (1999) find a value of $\sim 5 \times 10^{16}\,\mathrm{g\,s^{-1}}$ from their magnetic stripping model of the accretion flow in HU Aqr, which is comparable to the values deduced for $\sigma_9 = 1$. By comparison, the mass transfer rate expected if the orbital evolution is driven only by gravitational radiation is $\sim 7 \times 10^{15}\,\mathrm{g\,s^{-1}}$ (Faulkner 1971; Wickramasinghe & Wu 1994).

5.4 The wavelength dependence of the stream emission

One of the most remarkable features of the eclipse profiles of HU Aqr in both its high and low accretion states that the fraction of the overall system brightness due to the accretion stream is comparable to the brightness of the accretion region on the white dwarf. There is insufficient space in this paper to explore the emission mechanisms that could be causing the bright stream flux; these are discussed in Harrop-Allin (1999).

Clues regarding the emission processes operating in the stream can be deduced from the stream fluxes shown in Figs 4 and 6. The stream fluxes do not match a blackbody curve exactly, deviating in the U and R fluxes which fall significantly below a blackbody curve (i.e. the four-point 'spectrum' has too convex a shape to fit a blackbody curve). This is the case for both the two-footpoint and the one-footpoint geometry model results.

The stream fluxes in the various sections of the stream peak in B in most cycles and most stream sections (for both geometries); this is roughly consistent with a black-body of temperature 6500 K. We note that this temperature is of the same order of magnitude as that found by Liebert & Stockman (1985) for the magnetically-channeled part of the stream. The exceptions to this occur in the results from the two-footpoint geometry models. In four out of the five cycles in the two-footpoint geometry models, the stream sections on the magnetic part of the stream immediately adjacent to R_μ have fluxes that are consistent with a slightly higher blackbody temperature of 7400 K (blackbody curves with temperatures of 6500 K and 7400 K are shown for illustration in Fig. 4). The observed fluxes have not been corrected for reddening, either intrinsic to the system or interstellar in origin. If the fluxes are reddened significantly, the U-band fluxes will suffer the most, and our temperature estimates will be systematically too low.

If the two-footpoint model is the more accurate representation of the stream, and we accept that the stream fluxes can be characterized roughly by a blackbody, the four-point spectra of the stream sections imply that the stream material that has just been threaded at $\sim R_\mu$ is hotter than the fully-threaded plasma closer to the white dwarf and than the free-falling plasma before R_μ. We might expect there to be shock heating of the stream as it interacts with the magnetic field near R_μ: when the stream reaches the threading radius, the average kinetic energy per nucleon is $\sim$ 1–4 keV. Unless the threading process is extremely gentle, much of this energy will be converted into heat via a series of hydromagnetic shocks (Liebert & Stockman 1985, Hameury et al. 1986, Brainerd 1989). This might account for the elevated temperatures found in the stream just after R_μ.

6 CONCLUSIONS

We have applied the indirect imaging technique described in Paper 1 to *UBVR* eclipse profiles of HU Aquarii obtained when the system was in a high state of accretion. The eclipses are modelled using a stream consisting of a ballistic trajectory from the L1 point followed by a magnetically-channeled trajectory that follows a dipole field line out of the orbital plane. We use both a one-footpoint geometry, where the magnetically-channeled part of the stream follows the dipole field line onto only one footpoint of the dipole field line, and a two-footpoint geometry where the stream accretes onto both footpoints of the field line. We are not able to distinguish on statistical grounds which model provides the better fit to the data.

The stream images obtained using the two-footpoint geometry show no obvious dependence of brightness on radial distance from the white dwarf: instead, there are regions of the stream with localised brightness enhancements, particularly within the magnetosphere. Interestingly, there is no obvious brightening of the stream as it approaches either the the white dwarf or the coupling radius. The brightness enhancements in the magnetically-entrained sections of the stream may correspond to slow-moving pools of plasma in the magnetosphere. In the images from the one-footpoint geometry model, the stream brightens as it approaches the threading radius. It then fades as it is lifted out of the orbital plane, and brightens as it approaches the white dwarf. The brightest part of the stream in these models is not always closest to the white dwarf, but occurs about $0.08\,a$ from the white dwarf in several cycles in U and B.

The high state light curves of HU Aqr show a prominent pre-eclipse absorption dip in all wavebands. The centre of the dip moves to increasingly earlier orbital phases over the course of the observations, implying that the magnetically-entrained portion of the accretion stream moves from 42° from the line of centres at the beginning of the run to 48° at the end. This occurs without an accompanying change in the overall system brightness. The changes in R_μ found for the one-footpoint geometry models imply a reduction in the angle between the magnetically-entrained part of the stream and the line of centres from 42° to 47° during the observations, in close agreement with the results from the pre-eclipse absorption dip. This suggests that the one-footpoint model is the more appropriate for these data; the values of R_μ found using the two-footpoint geometry models do not change systematically during the run.

The models show that the ballistic stream is diverted to follow the magnetic field lines at a distance of $(1.0\text{–}1.3)\times10^{10}$ cm, corresponding to 17–21 white dwarf radii. Using the pre-eclipse absorption dip, the radius of the stream is estimated to be $\sim 3\times10^{9}$ cm. If we assume that the bulk of the stream is threaded where the ram pressure of the stream is balanced by the magnetic pressure of the white dwarf field, the mass transfer can be estimated; we find $\dot{\mathrm{M}}$ in the range $8\text{–}76\times10^{16}\,\mathrm{g\,s^{-1}}$ for the high accretion state.

In most sections of the stream, the flux peaks in B and is successively fainter in U, V and R; this is the case for *all* sections of the stream in the case of the one-footpoint models. In the two-footpoint models, however, the sections of the stream on the magnetically-channeled trajectory immediately adjacent to the threading radius have fluxes in U and B that are comparable in most cycles, suggesting that these sections of the stream are hotter than other parts of the stream. This may be due to shock heating of the plasma as it threads onto the magnetic field of the white dwarf, as suggested by Liebert & Stockman (1985), Hameury et al. (1986) and Brainerd (1989).

ACKNOWLEDGMENTS

We would like to thank Jon Mittaz and Chris Done for useful advice. MKHA acknowledges funding support from the Graduate School, University College London (Graduate Schools Research Scholarship), the Committee of Vice Chancellors and Principals of UK Universities (Overseas Research Student Award) and the University of Cape Town (Max & Lillie Sonnenberg Scholarship). PJH acknowledges the support of the Academy of Finland.

References

Allen C.W., 1973, Astrophysical Quantities. Athlone Press, London

Bailey J., 1995, in Buckley D.A.H., Warner B., eds, Cape Workshop on magnetic cataclysmic variables, ASP Conf. Ser. no. 85. ASP, California, p. 10

Bailey J., Cropper M., 1991, MNRAS, 253, 27

Barwig H., Ritter H., Barnbantner O., 1994, A&A, 288, 204

Brainerd J.J., 1989, ApJ, 345, 978
Diaz M.P., Steiner J.E., 1994, A&A, 283, 508
Faulkner J., 1971, ApJ, 170, L99
Glenn J., Howell S.B., Schmidt G.D., Liebert J., Grauer A.D., Wagner R.M., 1994, ApJ, 424, 967
Hakala P.J., Watson M.G., Vilhu O., Hassall B.J.M., Kellett B.J., Mason K.O., Piirola V., 1993, MNRAS, 263, 61
Hakala P.J., 1995, A&A, 296, 164
Hameury J.-M., King A.R., Lasota J.-P., 1986, MNRAS, 218, 695
Harrop-Allin M.K., 1999, Ph.D. thesis, Univ. of London
Harrop-Allin M.K., Hakala P.J., Cropper M., 1998, MNRAS, 302, 362 (Paper 1)
Heerlein C., Horne K., Schwope A.D., 1999, MNRAS, 304, 145
Hoard D.W., 1999, in Hellier C., Mukai K., eds, Proc. Annapolis Workshop on Magnetic Cataclysmic Variables, ASP, vol. 157, p. 201
Lampton M., Margon B., Bowyer S., 1976, ApJ, 208, 177
Liebert J., Stockman H.S., 1985, in Lamb D.Q., Patterson J., eds, Cataclysmic Variables and Low-Mass X-ray Binaries. Reidel, Dordrecht, p. 151
Lubow S.H., Shu F.H., 1975, ApJ, 198, 383
Marsh T.R., Horne K., 1988, MNRAS, 235, 269
Mukai K., 1988, MNRAS, 232, 175
Ramsay G., Wheatley P.J., 1998, MNRAS, 301, 95
Rosen S.R., Mason K.O., Cordova F.A., 1987, MNRAS, 224, 987
Schwope A.D., Beuermann K., Burwitz V., Mantel K.-H., Schwarz R., 1994, in Bianchini A., Della Valle M., Orio M., eds, Cataclysmic variables. Kluwer Academic Publishers, Dordrecht, p. 389
Schwope A.D. et al., 1998, in Howell S., Kuulkers E., Woodward C., eds, ASP Conf. Ser. 137, Proceedings of the 13th North American Workshop on CVs. ASP, California, p. 44
Schwope A.D., Mantel K.-H., Horne K., 1997, A&A, 319, 894
Schwope A.D., Thomas H.C., Beuermann K., 1993, A&A, 271, 25
Šimić D., Barwig H., Bobinger A., Mantel K.H., Wolf S., 1998, A&A, 115
Verbunt F., Heuvel E.P., van der Linden T.J., Brand J., van Leeuwen F., van Paradijs F., 1980, A&A, 86, L10
Warner B., 1995, Cataclysmic variable stars. Cambridge Univ. Press, Cambridge
Watson M.G., 1995, in Buckley D.A.H., Warner B., eds, Cape workshop on magnetic cataclysmic variables, ASP Conf. Ser. 85. ASP, California, p. 179
Watson M.G.,Rosen S.R., O'Donoghue D., Buckley D.A.H., Warner B., Hellier C., Ramseyer T., Done C., Madejski G., 1995, MNRAS, 273, 681
Wickramasinge D.T., Meggitt S.M.A., 1985, MNRAS, 214, 605
Wickramasinghe D.T., Wu K., 1994, MNRAS, 266, L1